# Internal Energy of Thermometer Ions Formed by Femtosecond Laser Desorption: Implications for Mass Spectrometric Imaging

Slobodan Milasinovic, Yang Cui, Robert J. Gordon, and Luke Hanley*

Department of Chemistry, M/C 111, University of Illinois at Chicago, Chicago, Illinois 60607-7061, United States

Ⓢ Supporting Information

ABSTRACT: Mass spectrometry (MS) imaging of biological samples would greatly benefit from improved lateral resolution and depth profiling which may be possible with femtosecond (fs), near-IR laser desorption microprobes to form ions directly in laser desorption ionization (fs-LDI) or via vacuum ultraviolet postionization (fs-LDPI). The use of fs-LDI-MS or fs-LDPI-MS for imaging, however, requires a determination of the magnitude of internal energy imparted by the ultrashort desorption pulse because the amount of internal energy determines the extent of ion fragmentation, and extensive fragmentation degrades MS imaging by complicating the mass spectra. This paper estimates internal energies imparted to 4-chlorobenzylpyridinium (CBP) thermometer ions desorbed from both simulated bacterial biofilms and bovine eye lens tissue samples by $\sim$75 fs, 800 nm laser pulses. Both direct ions and photoions formed by 10.5 eV single photon ionization of desorbed neutrals are analyzed by time-of-flight MS. Survival yields (SYs) of CBP varied from 0.2 to 0.8 and depended upon desorption laser fluence, overlap between desorption laser pulses, and whether direct ions or photoions were detected. SYs for photoions additionally depended on time delay between desorption and photoionization laser pulses, with the highest SYs seen at longer delay times. CBP internal energies were estimated using previously published computational results and compared with those from several other common MS imaging ion sources. The results are discussed in terms of their implications for MS imaging by fs-LDI and fs-LDPI.
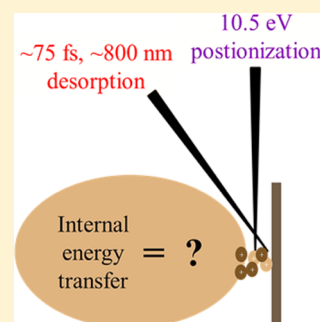
1. INTRODUCTION

Visualization of the spatial distributions of biomolecules in native biological samples such as animal tissue, microbial biofilms, or isolated cells by mass spectrometric (MS) imaging has received much attention over the past decade.[1−6] A variety of laser desorption-based MS imaging methods derived from nonimaging analysis of synthetic surfaces[7,8] have been used to detect both postionized species and ions formed directly from biological samples.[9] The amount of internal energy, E_{int}, imparted to a gaseous ion by laser desorption or any other desorption/ionization method determines the extent of its unimolecular dissociation and, consequently, the quality of chemical information available from MS analysis.[10] This paper estimates E_{int} imparted to thermometer ions desorbed from both simulated and actual biological samples by femtosecond (fs), near-IR laser pulses. Both direct ions and photoions formed by 10.5 eV single photon ionization of desorbed neutrals are analyzed by time-of-flight MS.

Laser desorption by sub-100 fs, $\sim$800 nm laser pulses offers advantages exploited in surgical[11−14] and bioengineering applications.[15,16] The energy from these ultrashort, near-IR laser pulses is absorbed by the substrate nonresonantly by a multiphoton mechanism. Optical absorption does not require a chromophore and occurs only in the focal volume. Furthermore, the short time scale of the desorption confines the thermal and mechanical energy, resulting in more precise removal of material and reduced radiation damage.[11,12] Ultrashort laser pulses are therefore potentially attractive

probes for MS imaging with high spatial resolution.[17−21] For example, MS imaging of onion epidermis using direct ions generated by fs laser desorption ionization (fs-LDI-MS) yielded images of the distributions of glucose and sucrose with a lateral resolution of $\sim$10 μm,[17] while $\sim$2 μm resolution was achieved for test targets.[21]

Postionization of desorbed species is often required, regardless of the characteristics of the desorption laser or whether desorption occurs in vacuum or under ambient conditions.[9] Ultrashort pulse laser desorption under ambient conditions followed by postionization of neutrals by electrospray has been used for both MS analysis[22] and imaging.[23] Several authors reported desorption of neutral species by ns UV laser pulses followed by 10.5 eV vacuum ultraviolet (VUV) single photon ionization[24] of neutral species in the plume. This method, known as laser desorption postionization (LDPI-MS), has been used for imaging of microbial biofilms.[9,25] The relatively "soft" single photon ionization of laser-desorbed neutrals by VUV photons in LDPI-MS yields singly charged radical cations. VUV single photon ionization coupled with $\sim$75 fs, $\sim$800 nm laser desorption in vacuum was also demonstrated for analysis, imaging, and depth profiling of endogenous small molecules in microbial biofilms (fs-LDPI-MS).[21]

The most widely used laser desorption method for MS imaging of biological samples is matrix assisted laser desorption/ionization (MALDI), which has been applied to a wide range of biomolecules.[1−4,9] MALDI nevertheless requires lengthy sample preparation and suffers from matrix ion interference and differential desorption/ionization yields.[26] The spatial resolution of MALDI is typically >25 μm, although values of ~5−10 μm have been achieved for some analyses with specialized experimental configurations.[27−29] Laser ablation electrospray ionization (LAESI) utilizes mid-infrared (2.94 μm) nanosecond laser pulses to overcome many of the disadvantages of MALDI, including the unsuitability of MALDI for depth profiling.[30] However, the lateral resolution of LAESI for MS imaging is ~30 μm under optimal conditions, and desorption efficiency varies with local water content.[30,31]

Both MALDI and LAESI are considered "soft" sources that produce ions with low E_{int}. The primary motivation for developing fs-LDI-MS and fs-LDPI-MS is their potential for achieving superior lateral resolution and improved depth profiling without the addition of a UV-absorbing matrix compound. The use of fs-LDI-MS or fs-LDPI-MS for imaging, however, requires a determination of the magnitude of E_{int} imparted by the ultrashort desorption pulse because the amount of internal energy determines the extent of ion fragmentation, and extensive fragmentation degrades MS imaging by complicating the mass spectra. MS imaging of molecular species therefore favors the use of soft ionization sources.

This study determines the magnitude of the E_{int} imparted into both direct ions and photoions generated by ~75 fs, ~800 nm pulses rastered across various sample surfaces. One such sample is a polyelectrolyte multilayer composed of alginate and chitosan polysaccharides, which were previously used to model a bacterial biofilm.[32] Both these multilayers and also bovine eye lens tissue were used as substrates, which were doped with the 4-chlorobenzylpyridinium (CBP) thermometer molecule. The laser fluence and raster parameters corresponded to typical MS imaging conditions. All estimates of E_{int} were made using experimentally measured survival yields (SYs) of CBP, which is known to fragment predominantly to a single benzyl cation fragment and a neutral pyridine.[33] CBP was chosen as a thermometer ion because of its frequent use in studies of energy transfer in MS ion sources.[33−38] The specific choice of CBP from the series of known substituted benzylpyridinium ions was made because its critical decomposition energy falls in the middle of the range for this series.[33] The effective values of E_{int}[10] were obtained by matching the calculated values of k_{RRKM}, the unimolecular rate constant calculated by Rice−Ramsperger−Kassel−Marcus (RRKM) theory, to experimental rate constants calculated from SYs measured here.[35,36] The use of only one thermometer ion also permitted a wider exploration of experimental parameters relevant to MS imaging. The results are discussed in terms of their implications for MS imaging of biological samples by ultrashort pulse laser desorption and compared with different desorption/ionization methods.

2. EXPERIMENTAL METHODS

2.A. 4-Chlorobenzylpyridinium Chloride Synthesis.
4-Chlorobenzyl chloride, anhydrous pyridine, acetonitrile, and diethyl ether were used as purchased (Sigma-Aldrich, St. Louis, MO). CBP chloride salt was synthesized by reflux at 80 °C in a slight excess of pyridine mixed with 4-chlorobenzyl chloride (1.2:1) in acetonitrile.[34] The product was cooled, filtered,

washed by diethyl ether, recrystillized twice, and validated with nuclear magnetic resonance spectroscopy.

2.B. Multilayer and Animal Tissue Section Preparation.
Gold coated silicon wafers (99.999% Au, layer thickness 1000 Å), cysteamine, gluteraldehyde, alginic acid sodium salt, and chitosan (low molecular weight) were all used as purchased (Sigma-Aldrich) for the multilayer preparation. The polyelectrolyte multilayers were deposited on top of gold-coated silicon wafers using cysteamine and gluteraldehyde as linkers to covalently bind the first layer of cationic polysaccharide chitosan, as previously described.[32] Anionic polysaccharide alginate and cationic chitosan were alternatively pipetted to prepare 10 bilayers of chitosan/alginate, corresponding to an ~80 nm thick multilayer.

Tissue sections of ~300 μm thickness were microtomed (Microme Vacutome/HM500OM, Thermo Scientific, Kalamazoo, MI) from bovine eye lens, as described previously.[20]

Approximately 125 μL of a 0.1 M aqueous solution of CBP chloride was pipetted over an ~1 cm^2 area of the multilayer chip or animal tissue section. These samples were then attached by a double sided adhesive tape to a MS sample plate and allowed to dry.

2.C. Description and Operation of the Mass Spectrometer.
Figure 1 is a schematic diagram of the home-built fs-
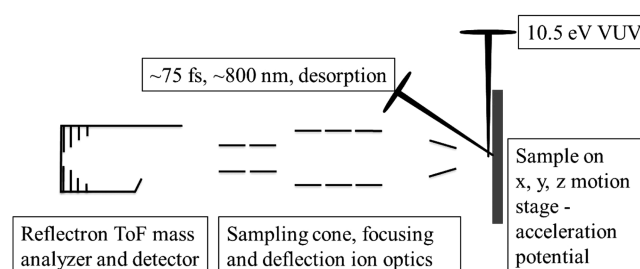
Figure 1. Schematic of femtosecond laser desorption postionization mass spectrometer (fs-LDPI-MS).

LDPI mass spectrometer described previously.[19,21] The desorption beam (~45 fs, ~800 nm) generated by a Ti:sapphire laser was passed through a 2× Galileo-type beam expander and focused onto the sample surface by an achromatic doublet lens (~200 mm focal length) at a 30° angle of incidence. The desorption laser had a spot diameter at the sample surface of ~30 μm, a Rayleigh range of ~100 μm, and the laser beam was s-polarized in all cases. A few experiments were performed with an objective lens (10× NA 0.28, Mitutoyo, Japan) at a 60° angle of incidence, producing a ~12 μm spot diameter and ~50 μm Rayleigh range. The spot radius, r, is defined as the radius at the e^{-2} point of the irradiance, measured by a scanning knife edge.[19] The focusing optics temporally stretched the pulses to ~75 fs, determined previously by an autocorrelation measurement. The energy of the desorption laser pulse (E, J) was measured with an energy/power meter (EPM2000, Coherent, Santa Clara, CA), from which the laser fluence (Φ, J/cm^2) was calculated using the relation $\Phi = 2E/(\pi r^2)$.

A 3D motion stage (PI miCos GmbH, Eschbach, Germany) having submicrometer positioning accuracy was used to move the sample. 10.5 eV (118 nm) VUV postionization laser pulses were generated from the 355 nm output of a Nd:YAG laser with ~5 ns pulse length (Tempest-10, New Wave Research, Portland, OR), using a home-built Xe/Ar harmonic generation

cell.[21,25] The time delay between the desorption and postionization pulses and pulsed deflection optics was controlled using a digital delay generator (DG535, Stanford Research Systems, Sunnyvale, CA). Ion optical parameters in the ion source critical for the analysis of survival yields were kept constant in all experiments. The continuous extraction voltage was 3.7 kV, while the sampling cone was kept at 0.6 kV. The mass analyzer consisted of Einzel lenses, deflectors with pulsing capability, and a two-stage reflectron time-of-flight drift tube and detector (model 31374, Photonis, Lancaster, PA). The instrument control and data acquisition software was developed in-house (LabVIEW, National Instruments, Austin, TX).[21]

Two modes of operation were used: analysis of positive ions produced directly by femtosecond laser desorption ionization (fs-LDI) or by single photon VUV postionization of femtosecond laser desorbed neutrals to form photoions (fs-LDPI). fs-LDI experiments were performed without the use of the VUV source, and only ions formed directly during the desorption event were analyzed in this mode. fs-LDPI-MS was performed by measuring photoions produced by the VUV laser pulse from the neutrals in the plume, while a pulsed deflector (+400 V) was used to deflect all direct ions. The deflector was turned off 1 μs before the VUV pulse to allow detection of the photoions. All experiments were performed under vacuum at a 10 Hz repetition rate, while the desorption laser fluence and scanning speeds were varied across experiments. No attempts were made to detect negative ions because prior work has not attempted their detection.

The fs-LDPI-MS experiments were performed by rastering the desorption laser across the sample surface. To increase the ion signal in these experiments, either the laser fluence could be increased or the laser scanning speed could be decreased to achieve oversampling by overlapping individual laser shots on the surface. The degree of laser beam spot overlap (O_d) as a function of raster scanning speed (s), laser spot diameter at the sample surface (d_l), and the laser pulse frequency (f_p) is given by[39]

$$O_d = 1 - \frac{s}{d_l f_p} \tag{1}$$

The authors previously reported that the ion signal intensities of various endogenous species increased 3−10 times in the analysis of animal tissue from previously ablated areas, compared with native, unablated tissue.[20] These increased ion yields might have resulted from enhanced desorption from laser-ruptured tissue. This speculation led to an investigation of whether analysis under oversampling conditions would affect E_{int} as compared to no oversampling, since the degree of overlap controls the extent to which consecutive laser shots sample material from a previously ablated region of the surface. Experiments contrasting two limiting cases corresponding to laser beam overlap of $O_d = 0$ and $O_d = 0.9$ are referred to below as "zero overlap" and "high overlap," respectively.

2.D. Calculation of Survival Yields and Experimental Unimolecular Decay Rate Constants. SYs were calculated from the ratio of precursor and fragment ions of the thermometer ion, CBP. The precursor and fragment peak areas were analyzed using a peak analysis tool in commercial software (Origin Pro 9.0, OriginLab, Northampton, MA). SYs were calculated using data collected at laser fluences

immediately above the ion appearance thresholds up to fluences where the spectral resolution was observed to deteriorate and/or there was no appreciable gain in ion signal. To obtain good statistics, individual spectra were averaged over 500 laser shots, and at least five spectra per data point were collected. This number of laser shots was chosen as the most that could be recorded from a given sample size at zero overlap. Larger samples would have allowed more laser shots per samples but also would have required recording mass spectra with different ion optical voltages which might have introduced an unwanted variability in the ion collection efficiency. A Student's t test was performed to validate the calculated SYs, and only points within the 95% confidence interval were included in the average. Ion intensities were calculated as peak areas of the monoisotopic precursor, M^+, and fragment, F^+, ions. Absolute ion intensity analyses were complicated by fluctuations in ion signal from shot to shot and from day to day due to contributions from both desorption and postionization lasers and the sample inhomogeneity. By contrast, SY analyses employed ion intensity ratios that gave very reproducible and stable results.

Experimental unimolecular decay rate constants were calculated using the measured SYs and the time, τ, that ions remain in the acceleration region of the mass spectrometer (see below). The value of τ was estimated from the source geometry, ion optical parameters, and assumptions made about initial ion velocities based upon prior work.[40−42] The distance between acceleration potential electrode and the sampling cone in the source was 10 mm. The acceleration and sampling cone potentials were 3.7 and 0.6 kV, respectively, and were held constant throughout all experiments. The path that direct ions traveled through the ion source was taken to be the full distance of 10 mm, while it was estimated to be 6 mm for photoions generated from the expanding plume. The electrostatic field between the acceleration plate and the sampling cone was assumed to be uniform. Initial velocities of direct and photoions were assumed to be 500 and 100 ms^{-1}, respectively. The electrostatic field strength and ion acceleration potential were used to calculate that the thermometer ions required a τ of 280 ns for direct ions and 360 ns for photoions to exit the ion source. Estimates of E_{int} barely changed across this range of τ, which was subsequently set to 300 ns in all cases.

3. RESULTS

3.A. Mass Spectra of Thermometer Ions. The CBP ion undergoes unimolecular decomposition corresponding to a loss of neutral pyridine moiety.
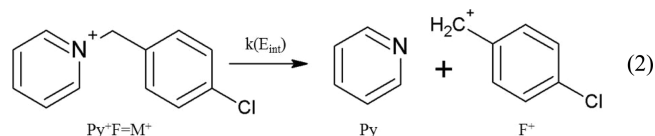

$$\tag{2}$$

Figure 2 presents mass spectra obtained under sampling conditions of zero overlap of the laser desorption spot from the CBP salt doped into either a multilayer or animal tissue sample. (See Supporting Information for "high overlap" spectra.) The thermometer ion precursor M^+ at m/z 204 and its dominant fragment F^+ at m/z 125 each displayed the expected $^{35}Cl/^{37}Cl$ isotopic patterns in all spectra.

A direct ion spectrum obtained from a multilayer sample at a laser fluence of 0.32 J/cm^2 is shown in Figure 2a, collected without any VUV postionization. Accordingly, the internal

28940

dx.doi.org/10.1021/jp504062u | J. Phys. Chem. C 2014, 118, 28938−28947
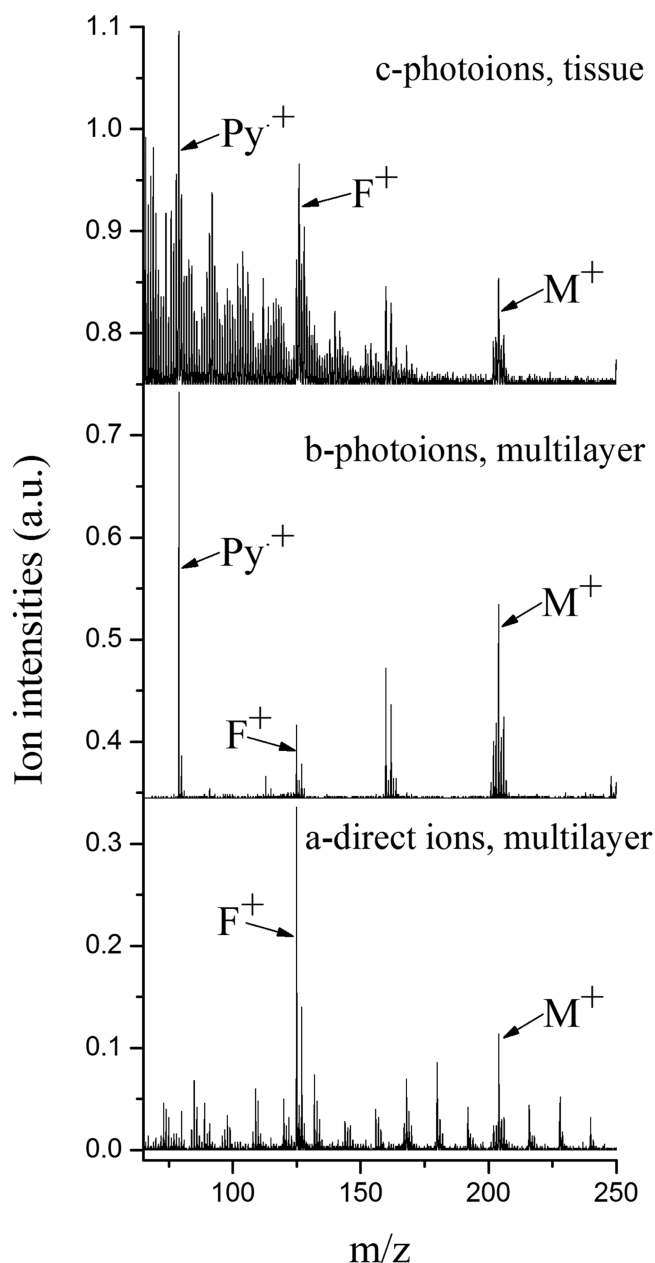
Figure 2. Mass spectra of 4-chlorobenzylpyridinium (CBP) thermometer ions obtained under zero overlap conditions: (a) direct ions sampled from multilayer at desorption laser fluence of 0.32 J/cm^2; (b) photoions sampled from multilayer at fluence of 0.90 J/cm^2; (c) photoions sampled from tissue section at fluence of 1.0 J/cm^2. M$^+$ is a precursor thermometer ion. F$^+$ is benzyl cation fragment. Py$^{\bullet+}$ is a pyridine radical cation.

energy of the thermometer ions is derived almost entirely from energy imparted by the desorption laser. Direct ion spectra were dominated by thermometer precursor and fragment ions, as expected. Various species were also detected in the direct ion spectra, which presumably arose from depolymerization of the chitosan and alginate biopolymers comprising the multilayer.

Figure 2b displays photoions obtained from the multilayer sample at desorption laser fluence of 0.90 J/cm^2, with a 20 μs delay between desorption and VUV postionization pulses. The photoion spectra were much simpler in appearance than the direct ion spectra. Since all direct ions were intentionally deflected, no signal could be detected when the VUV source

was blocked (data not shown), ensuring that all detected ions corresponded to photoionized neutrals. The photoion spectra were also dominated by the thermometer precursor and fragment ions but also included the pyridine radical cation Py$^{\bullet+}$ at m/z 79 which was not observed in the direct ion spectra. Py$^{\bullet+}$ was not considered in the data analysis below because it was not observed in the direct ion spectra, it could have formed by VUV single photon ionization from the neutral pyridine product of unimolecular decomposition of deflected direct CBP ions (i.e., from laser desorption only), and it was not observed by other published experiments.

Figure 2c presents the spectrum of photoions recorded at 1.0 J/cm^2 fluence from a bovine eye lens tissue section doped with CBP. This spectrum is also dominated by thermometer precursor and fragment ions. Figure 2c differs, however, from the multilayer spectrum, having a high density of peaks below m/z 170 that presumably are derived from components of the tissue. Figure 2c also displays the Py$^{\bullet+}$ ion. Direct ion analysis from the tissue sections was attempted but did not yield a detectable signal for the thermometer ions.

There are a few obvious qualitative differences between spectra acquired under zero overlap and high overlap conditions (see Supporting Information). Generally, the ion intensities increased with laser fluence, and for multilayer samples high overlap conditions gave greater ion intensities than zero overlap. The extent of laser overlap did not affect photoion intensities from tissue samples, which in any case were lower than those obtained from the multilayers. Overall, ion intensities observed under different experimental conditions were within an order of magnitude of each other. In all subsequent analyses, it was assumed that there were no substrate-related species overlapping with the dominating M$^+$ and F$^+$ ion signals and that no alternative fragmentation routes were present.
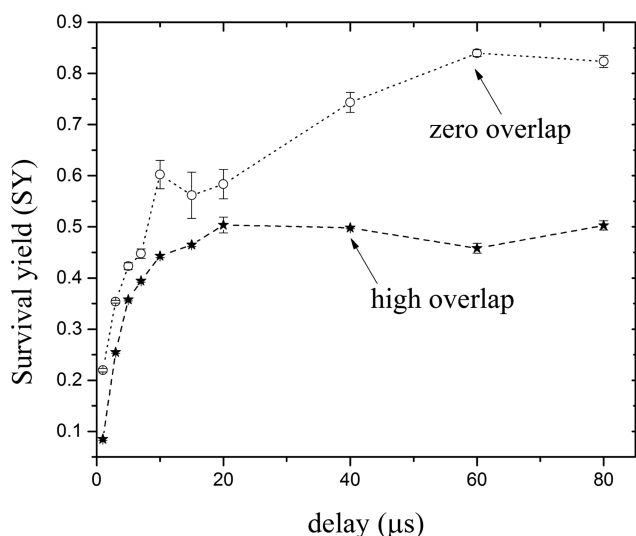
3.B. SYs of Photoions from Multilayers vs Desorption−Photoionization Delay. Survival yields of the CBP thermometer ions were calculated by eq 3,

$$SY = \frac{I(M^+)}{I(M^+) + I(F^+)} \qquad (3)$$

where $I(M^+)$ is the area of the monoisotopic peak corresponding to the precursor ion at m/z 204, and $I(F^+)$ is that of the fragment ion at m/z 125. Figure 3 shows that the SYs of photoions produced from multilayer samples increased with the delay between desorption and postionization laser pulses. The increase in SYs with delay time was observed for both zero overlap in adjacent laser pulses and high overlap. Maximum SYs of ∼0.5 for high overlap and ∼0.8 for zero overlap were observed at a 60 μs delay.

One observation not apparent from in the figures is that absolute ion signal decreased with delay between the desorption and postionization laser pulses. Although the SY increased with delay, long delay times were not useful because of the decline in ion signal. Optimal delays were found to lie between 20 and 40 μs. A 20 μs delay was used in all subsequent postionization experiments as the optimal trade-off between ion intensity and SY.[21]

3.C. SY vs Laser Fluence of Direct and Photoions from Multilayer Samples. Figure 4 displays the dependence of the thermometer ion SY from multilayer samples on desorption laser fluence (J/cm^2) under both zero and high laser overlap (panels "a" and "b", respectively). The appearance thresholds

Figure 3. SY of photoions analyzed from multilayers as a function of desorption/postionization time delay (μs): stars, high desorption overlap ($O_d = 0.9$); open circles, zero desorption overlap ($O_d = 0$).
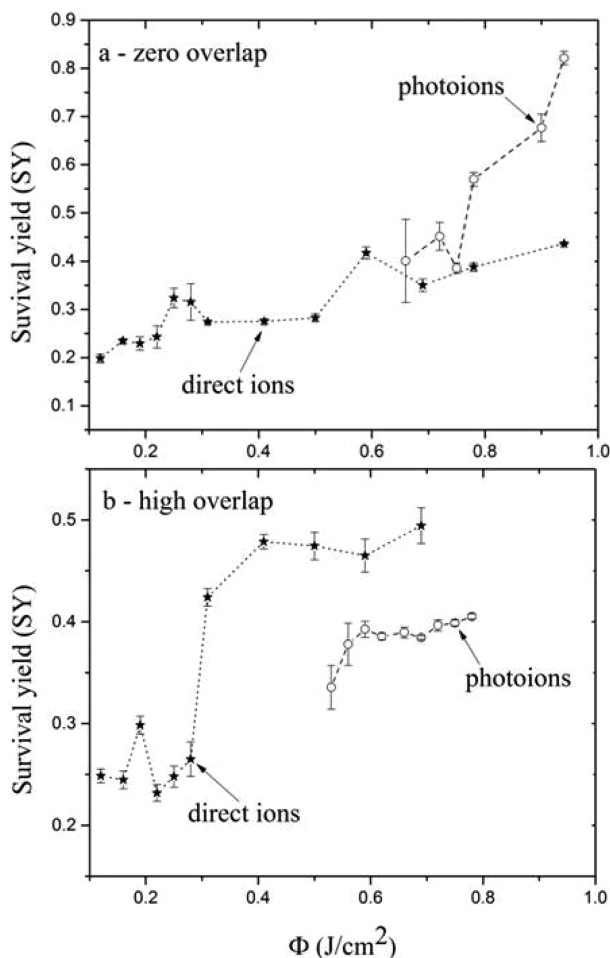
Figure 4. SY of ions analyzed from multilayers as a function of desorption laser fluence (J/cm^2): stars, direct ions; open circles, photoions; (a) zero desorption overlap; (b) high desorption overlap.

for photoions were 4−5 times higher than those of direct ions. All SYs increased with laser fluence, both for zero and high overlap. Photoions analyzed under zero overlap conditions

were internally cooler than direct ions under both overlap conditions, with the SY steeply increasing up to ~0.8 for a laser fluence of ~0.9 J/cm^2 at zero overlap and ~0.4 at high overlap. Data could not be collected from multilayers at laser fluences above ~1 J/cm^2 due to MS peak broadening.

The desorption mechanism of the thermometer molecules from the ~80 nm thick multilayers on Au-coated Si wafer may be dependent on the interplay between laser fluence and overlap. The appearance of Au ions in the spectra (data not shown) from the underlying substrate corresponded to some extent with jumps in SY values for the direct ions. Specifically, Au^+ ions at m/z 197 began to appear in direct ion spectra at desorption fluences of ~0.6 J/cm^2 for zero overlap and ~0.4 J/cm^2 for high overlap.

3.D. SY of Photoions from Animal Tissue. Additional experiments used ~300 μm thick animal tissue sections from bovine eye lens, which were previously characterized in terms of the desorption rate dependence on the laser fluence.[20] On the basis of that earlier work, it was assumed that under the experimental conditions applied here, optical absorption of ultrashort pulse laser energy and the subsequent material desorption and E_{int} energy transfer resulted solely from the interaction of tissue with the laser, without any effect from the substrate upon which the tissue section was mounted. The tissue sections were therefore assumed to better simulate true biological samples used in practical MS imaging by reducing the impact of potential interference from the inorganic substrate on which the ~80 nm thick multilayers were prepared.

Only photoions could be detected from the tissue sections, as shown in Figure 5; attempts to analyze direct ions under
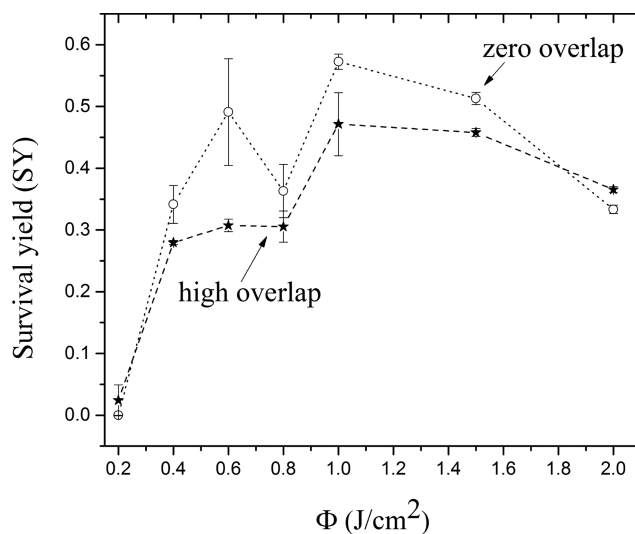
Figure 5. SY of photoions analyzed from tissue section as a function of desorption laser fluence (J/cm^2): stars, high desorption overlap; open circles, zero desorption overlap.

comparable ion optical parameters were unsuccessful (data not shown). The ~0.20 J/cm^2 appearance thresholds of photoions from tissue were lower than from the multilayers and are consistent with the previously reported value of 0.14 J/cm^2 recorded for tissue under ambient conditions for identical tissue sections under otherwise similar conditions.[20]

Figure 5 displays the fluence dependence of the SY of photoions produced from tissue sections under zero and high overlap conditions. The SY is seen to increase monotonically

with desorption laser fluence until reaching a plateau at ~1.0 J/cm^2. Similar to results obtained from multilayer samples, SYs under zero overlap conditions were slightly higher than for high overlap conditions. The peak value of the SY was ~0.5 for high overlap and ~0.6 for zero overlap. Further increase of laser fluence caused the SY to decrease in both cases.

3.E. Estimates of E_{int}. The experimental unimolecular rate constant, k_{exp}, was calculated from the survival yields using the expression[33,36]

$$k_{exp} = -\frac{1}{\tau}\ln(\text{SY}) \tag{4}$$

The constant τ corresponds to the time that ions spend in the acceleration region of the mass spectrometer and was set to 300 ns for all cases (see Experimental Methods). The value of E_{int} was then deduced by comparing k_{exp} with the theoretical calculation of the internal energy dependence of k_{RRKM}[36] given by[10] (see Supporting Information)

$$k_{RRKM} = \frac{\sigma G^*(E_{int} - E_0)}{h\rho(E_{int})} \tag{5}$$

Two separate RRKM calculations of k_{RRKM} for CBP[35,36] were used to obtain estimates of E_{int} for the thermometer ion (see Supporting Information). The RRKM plot from ref 36 was used to compare the E_{int} values determined here with those reported for MALDI and silicon-nanoparticle assisted laser desorption/ionization (SPALDI), while the RRKM plot from ref 35 generated different results based on recalibrated values of vibrational frequencies and critical energy, E_0.

Table 1 summarizes the estimates of E_{int} for the thermometer ion based on different experimentally determined SYs. The

Table 1. Estimates of E_{int} of CBP Thermometer Ion Based upon Experimental SY and Theoretical Predictions from Refs 36 and 35

SY	k_{exp}	$\log(k_{exp})$	E_{int} (eV) (ref 36)	E_{int} (eV) (ref 35)
0.20	5.4×10^6	6.73	4.3	5.8
0.50	2.3×10^6	6.36	4.1	5.5
0.80	7.4×10^5	5.87	3.8	5.2

lowest and highest SYs observed here were ~0.20 and ~0.80, although the value of ~0.50 was often observed; all three values were used to calculate k_{exp}. These values of the rate constant were then used to extract E_{int} from the theoretical plots of the energy dependence of k_{RRKM}. The values of E_{int} extracted using k_{RRKM} from ref 36 were lower than those obtained using ref 35. In the former case, E_{int} values range from ~3.8 to ~4.3 eV, corresponding to a range of SY from ~0.80 to ~0.20, respectively, while in the latter case, E_{int} values range from ~5.2 to ~5.8 eV.

4. DISCUSSION

4.A. Energy Transfer during Femtosecond Laser Desorption. Survival yields of the thermometer ions depended on several experimental variables for both direct ions produced from multilayer samples and photoions formed by single photon ionization from both multilayer and tissue samples. The SYs increased with desorption laser fluence for all ions, and ion appearance thresholds were significantly lower for direct ions than for photoions. Similar trends were observed from both multilayers and animal tissue, although only photoions were

detected from tissue. SYs of photoions from multilayers also increased with the time delay between desorption and photoionization laser pulses. Rastering the desorption laser with zero overlap on the sample yielded greater values of SY compared to high laser spot overlap.

The energy from ultrashort 800 nm desorption laser pulses is absorbed by the multilayer and tissue samples via a non-resonant multiphoton mechanism.[11,12] Optical breakdown under sufficiently high laser fluence leads to a plasma-mediated Coulombic explosion that drives the material desorption. The literature value of the irradiance threshold for the optical breakdown of water and transparent biological materials is ~10^{13} W/cm^2.[11] Desorption below this threshold can also occur by superheating of the matrix to cause a phase explosion.[18]

Photoions are excited internally by both desorption and postionization laser pulses. The SYs of the photoions increased with time delay[43] (see Figure 3), with the longest delays leading to the largest SY value of 0.8, albeit at rather low ion intensities. A complicating issue is the observation that femtosecond laser desorbed material can include atoms, molecules, ions, clusters, nanoparticles, small droplets, and particulates, which expand into vacuum with a wide range of velocities.[40−42] An experimental study employing ~25 fs, ~800 nm laser desorption and postionization of neutrals ablated from bone argued that an abundance of clusters ejected at ~30−600 m/s velocity dissociated upon postionization to produce small ions observed at $m/z < 100$.[42] The thermometer photoions observed here might be similarly generated from clusters in the desorbed plume, as also observed for nanosecond laser desorbed clusters.[32] These considerations complicate the quantification of energy transfer imparted to the thermometer photoions by 10.5 eV VUV photons, unlike the case of single photon ionization of gaseous neutrals.[24,43]

Additionally, it was found that SYs increase with laser fluence for both multilayers and tissue sections (see Figures 4 and 5, respectively). A ~10^{13} W/cm^2 threshold for optical breakdown and plasma-mediated ablation in biological materials[11] corresponds roughly to a laser fluence of 0.7 J/cm^2 for 75 fs pulses. Analysis of multilayers for zero overlap conditions showed a slight increase in the SY of direct ions from ~0.2 to ~0.4 as the laser fluence increased. Similarly, SYs of photoions from tissue sections reached their maximal values above 0.7 J/cm^2, rising from ~0.3 at 0.4 J/cm^2 to ~0.6 at 1.0 J/cm^2 in the case of zero overlap and from ~0.3 to ~0.5 for high overlap. A prior study of nanosecond UV laser desorption displayed a linear decrease in translational temperature of molecules in the laser plume with increasing desorption laser peak power, which was attributed to enhanced collisional cooling caused by a greater number of intermolecular collisions in the desorption plume.[43] This result is in agreement with computational simulations of laser ablation of molecular substrates by short pulses, which showed an increase in ablation rate with laser fluence that was initially driven by a thermal process.[44] However, the tissue results in Figure 5 indicate that SYs of photoions decreased again past the assumed optical breakdown threshold, indicating that optimal conditions for probing by ultrashort laser pulses are at or slightly higher than the assumed threshold for optical breakdown. Prior observations that E_{int} of ions from MALDI and SPALDI usually increased continuously with laser desorption fluence[36,45,34] indicate fundamental mechanistic differences compared to fs-LDI and fs-LDPI.

Table 2. Review of SY and E_{int} of 4-Chlorobenzylpyridinium Ion Reported for Various Ion Sources

ref	technique	method	SY	E_{int} (eV)
37	DESI	original SY method[a]	∼0.45−0.75[b]	1.9
38	LAESI (from plant tissue)	original SY method[a]		1.98 ± 0.65[c]
34	SPALDI	simplified SY method[36]	0.3−0.95	2.8−3.7[d]
36	MALDI	simplified SY method	>0.88[e]	3.69 ± 0.21[e]
	fs-LDPI and fs-LDI	simplified SY method	0.2−0.8	3.8−4.3 (5.2−5.8 when ref 35 data used)
35	nanocluster SIMS	E_{int} distribution = (rate distribution estimated from ToF data) × (recalibrated RRKM curve)	∼0.43	6.414 ± 2.0%[f] (∼5.0 if data from ref 36 used)

[a]These are not absolute values of E_{int} and do not include kinetic shift. E_{int} is the mean of Gaussian distribution. See ref 33. [b]For heated capillary inlet biased between 70 and 100 V. [c]For 60 V potential difference between sampling and skimmer cone. [d]Energy transfer depends on applied nanoparticles. E_{int} given is actually "effective energy". [e]Energy transfer depends on applied matrix. Value given for α-cyano-4-hydroxycinnamic acid matrix. E_{int} is actually "effective energy". [f]E_{int} is given as the most probable value within the distribution.

Figure 4 b displays the fluence dependence of SYs under high overlap conditions. For direct ions, a more rapid increase of SYs with fluence was observed, which occurred at lower fluences than for the case of zero overlap. For photoions, the appearance threshold was lower for high overlap, and almost no increase of SY with fluence was observed. This observation may have arisen when the desorption laser was rastered at high overlap across the ∼80 nm thick multilayers.[32] Under high overlap, each laser shot desorbed from a multilayer area that is only ∼10% intact so that the remaining 90% of the laser spot desorbed from a previously ablated area where the underlying Au-coated substrate was already exposed. Thus, high overlap is closer to desorption from a metallic surface than zero overlap that sampled predominantly intact multilayers. Furthermore, metallic surfaces may be more readily ablated; the theoretically calculated threshold for plasma mediated ablation of Au is ∼0.4 J/cm² for 800 nm, ∼100 fs pulses,[46] lower than the ∼0.7 J/cm² threshold for biological material observed here.

Analysis of the SYs of photoions from both multilayers and tissue sections (Figures 4 and 5) indicated that the SYs tended to be higher for zero overlap than for high overlap. One possible explanation for such behavior is that the tissue tensile strength was compromised by previous laser shots under high overlap.[18,20] Assuming the desorption arises from the combination of photothermal and photomechanical effects,[11] the latter may be more prominent under zero overlap, since a pressure build-up and phase explosion may occur more rapidly within the constraints of intact tissue, allowing for less energy to be transferred into ions before the material ejection takes place (compared to high overlap). While thermal accumulation may also play a role here, thermal accumulation manifested as thermal damage by ultrashort laser pulses was observed previously only for >100 Hz repetition rates[47,48] (vs 10 Hz employed here).

Direct ions could not be detected from the tissue samples. Furthermore, the highest SYs of direct ions from multilayers did not exceed ∼0.5, whereas analysis of photoions yielded SYs exceeding ∼0.8 in some cases. These results support the use of VUV single photon ionization, especially when considering that neutral material ejection dominates during laser desorption.[9,24,42]

4.B. Energy Transfer by Femtosecond Laser Desorption vs Other Ion Sources Used for MS Imaging. Table 1 summarizes the ∼0.2 to ∼0.8 SYs observed here for fs-LDI and fs-LDPI and the corresponding E_{int} of CBP ions. Table 2 compares a summary of these results with E_{int} of CBP ions obtained by various other ion sources employed in mass spectrometric imaging, although several of those results were

determined via different methods (noted therein). The most relevant and direct comparison can be made with MALDI data obtained from ref 36, which employed the same simplified survival yield method as was used here. The SY and E_{int} results for fs-LDPI-MS are comparable to the MALDI data. An average E_{int} of ∼3.7 eV was reported for MALDI using the "softest" of the three matrix compounds investigated therein. This MALDI value is comparable to the lowest value obtained by fs-LDPI reported here, corresponding to photoions analyzed at a higher time delay between desorption and postionization observed at a desorption laser fluence of >0.7 J/cm² (under zero overlap conditions), which was estimated to be ∼3.8 eV at SY of ∼0.8. The internal energy of triacontane, calculated from desorption by 349 nm, 7 ns pulses and VUV single photon ionization, was reported to be 4.6 eV,[43] in relative agreement with the lower set of values of E_{int} estimated here for CBP ions by fs-LDPI-MS (although ref 43 used an entirely different strategy to estimate E_{int}).

Direct comparison can also be made with data corresponding to nanocluster secondary ion MS reported in ref 35 (see next section). The ∼6.4 eV E_{int} reported in that study is well above the ∼5.8 eV E_{int} estimated for fs-LDPI-MS using the RRKM calculations reported therein. Note that the offset of ∼1.4 eV between the two sets of estimated E_{int} values reported in Table 1 arises from differences in the RRKM calculations used in each case, as discussed further below.

Table 2 also contains values of E_{int} measured for thermometer ions produced by laser ablation electrospray ionization (LAESI)[38] and desorption electrospray ionization (DESI).[37] In both cases, a direct comparison on the same instrument between LAESI, DESI, and ESI-only produced ions indicated that E_{int} of thermometer ions from both LAESI and DESI was determined predominantly by the ESI step, not the desorption step.[37,38] Nevertheless, the E_{int} values from all three ESI-based methods are not absolute, since they were obtained by the original survival yield method and cannot be directly compared to values determined by the simplified survival yield method (see below).

4.C. Evaluation of Method for Determining E_{int}. The simplified survival yield method employed here[36] does not make the same assumptions about the nature of internal energy distributions (e.g., thermal or nonthermal) and sigmoidal relationship between SY of thermometer ions and critical energy (E_0 in eq 5) as made in the original survival yield method.[33] The simplified survival yield method also accounts for the time scale of the experiment and extracts estimates of E_{int} of thermometer ions using the experimental rate constants, k_{exp}. Rather than using a E_{int} distribution curve, results are

represented by the "effective" value (the internal energy that gives the same result in an experiment as the actual internal energy distribution).[10] This approach allows for use of a single thermometer ion and simplifies the experimental design and data representation. In addition, the expected ratio of the SY for the CBP ion to that of the more fragile 4-methoxybenzylpyridinium ion was verified experimentally here (data not shown).

The use of a time-of-flight mass analyzer facilitated estimation of the time scale for unimolecular dissociation. Although the SYs reported here do not take into account the potential for postsource decay of the thermometer ions, no metastable peaks were observed. (Such postsource decay would have produced broadened peaks at anomalous mass values.) As a consequence, abundances of M^+ ions measured can only be lower than the actual abundances exiting the ion source, while corresponding abundances of F^+ ions would remain unaffected. Hence, the SY values measured here are potentially lower, and consequently the E_{int} estimates are likely to overestimate actual values. Under all experimental conditions applied, both M^+ and F^+ ions could be detected, which in addition to the observed high abundance of $Py^{\bullet+}$ in the photoion spectra indicates that decay of thermometer ions occurs within ~300 ns and that the choice of method and thermometer ion is appropriate.

The values of E_{int} deduced from the measured survival yields depend on the properties of the ground state and transition state of the excited molecule. In particular, the calculated value of k_{RRKM}[35,36] is sensitive to the methods used to obtain the critical energy, E_0, and the vibrational frequencies used to calculate G^* and ρ in eq 5. The ~1.4 eV difference between the E_{int} values reported in Table 1 is due at least in part to the different values of E_0 used in refs 35 and 36 (2.375 vs 1.73 eV) and to different levels of theory employed for molecular orbital calculations of vibrational frequencies used in the RRKM calculations.[49]

5. CONCLUSIONS

This work was motivated by the possibility of using ultrashort, mid-IR laser pulses for MS imaging with greater spatial and depth resolution.[18,20] Such improvement stems from the precise removal of surface material with minimal thermal and mechanical side effects. Obtaining this precision requires localization of energy deposition during the laser pulse, which can be achieved by high numerical aperture optical lenses[21] and/or by nonlinear absorption.[20] Nonlinear absorption and thermal and stress confinement are readily achieved by sub-100 fs laser pulses, in contrast to nanosecond pulse lengths. First, the mathematical expressions used to describe thermal and stress confinement indicate that these favorable phenomena are enhanced at this wavelength.[11] Second, the small linear absorption coefficient at 800 nm wavelength renders most biological tissues virtually transparent, reducing photochemistry.[11] Hence, the use of ~75 fs, ~800 nm laser pulses continues to show great promise for biological MS imaging with high spatial and depth resolution.[17−21]

The internal energy content of thermometer ions produced by the ultrashort pulse laser desorption was measured both with and without VUV postionization. Internal energy transfer was estimated for both fs-LDPI and fs-LDI (photoions and direct ions) using experimental conditions appropriate for MS imaging of tissue. In all cases, energy transfer could be controlled by varying desorption laser fluence, laser raster rate, and in the case of fs-LDPI, desorption/postionization delay. The E_{int} values observed (Table 1) are comparable to other laser desorption-based MS imaging techniques, namely, MALDI-MS and LDPI-MS, and lower than those reported for nanocluster-SIMS (Table 2), arguing that ultrashort pulse laser desorption can be used as a probe in "soft" MS imaging ion sources, at least under the probe laser conditions examined here.

Use of a high focusing power objective lens (data not shown) was hampered by a very low S/N ratio, and for this reason all results presented here were collected using a ~30 μm desorption laser spot diameter. The potential for high resolution MS imaging comes at a cost of lower detection limits under high focusing conditions, but this is the same situation with MALDI.[50] The ~30 μm spatial imaging resolution that would correspond to the experimental conditions used here[21] and the low internal energy transfer are certainly encouraging and argue for a high potential of fs-LDI-MS and fs-LDPI-MS for MS imaging applications. Future improvements in fs-LDI and fs-LDPI are planned that will utilize a higher collection efficiency ion source that should improve detection limits at smaller laser spot diameters. Furthermore, instrumental design improvements could facilitate operating the fs-LDPI at higher values of desorption/postionization time delay, where SYs of thermometer ions approach unity. These improvements should permit fs-LDPI-MS imaging with superior spatial imaging resolution and "soft" ion generation coupled with minimal sample preparation.

Estimates of E_{int} reported here were made using RRKM calculations of the unimolecular decomposition rates. The accuracy of these calculations depends on the methods used to calculate the critical energy (E_0) of the decomposition reaction and the vibrational frequencies of the ground and transition states of thermometer ions.[10,35,36] An ~1.4 eV shift in E_{int} was observed for different values of E_0 and vibrational frequencies used to calculate k_{RRKM}.[35] It is therefore presumed that the previously cited values of E_{int} for MALDI-MS and SPALDI-MS (Table 2) would have been similarly shifted if calculated with the recalibrated data.

■ ASSOCIATED CONTENT

ⓢ Supporting Information

Mass spectra under high overlap conditions and further discussion of the determination of internal energy from unimolecular dissociation rate constants calculated from RRKM theory. This material is available free of charge via the Internet at http://pubs.acs.org.

■ AUTHOR INFORMATION

Corresponding Author

*E-mail: LHanley@uic.edu. Phone: +1-312-996-0945.

Notes

The authors declare no competing financial interest.

■ ACKNOWLEDGMENTS

■ REFERENCES

(1) Amstalden van Hove, E. R.; Smith, D. F.; Heeren, R. M. A. A Concise Review of Mass Spectrometry Imaging. *J. Chromatogr., A* **2010**, *1217*, 3946−3954.

(2) Watrous, J. D.; Alexandrov, T.; Dorrestein, P. C. The Evolving Field of Imaging Mass Spectrometry and Its Impact on Future Biological Research. *J. Mass Spectrom.* **2011**, *46*, 209−222.

(3) Trouillon, R.; Passarelli, M. K.; Wang, J.; Kurczy, M. E.; Ewing, A. G. Chemical Analysis of Single Cells. *Anal. Chem.* **2012**, *85*, 522−542.

(4) Seeley, E. H.; Caprioli, R. M. 3D Imaging by Mass Spectrometry: A New Frontier. *Anal. Chem.* **2012**, *84*, 2105−2110.

(5) Fletcher, J. S.; Vickerman, J. C. Secondary Ion Mass Spectrometry: Characterizing Complex Samples in Two and Three Dimensions. *Anal. Chem.* **2013**, *85*, 610−639.

(6) Wu, C.; Dill, A. L.; Eberlin, L. S.; Cooks, R. G.; Ifa, D. R. Mass Spectrometry Imaging under Ambient Conditions. *Mass Spectrom. Rev.* **2013**, *32*, 218−243.

(7) Land, D. P.; Wang, D. T. S.; Tai, T.-L.; Sherman, M. G.; Hemminger, J. C.; McIver, R. T., Jr. Postionization of Laser-Desorbed Neutrals for the Analysis of Molecular Adsorbates on Surfaces. In *Lasers and Mass Spectrometry*; Lubman, D. M., Ed.; Oxford University Press: New York, 1990; pp 157−178.

(8) Lykke, K. R.; Parker, D. H.; Wurz, P.; Hunt, J. E.; Pellin, M. J.; Gruen, D. M.; Hemminger, J. C. Mass Spectrometric Analysis of Rubber Vulcanizates by Laser Desorption/Laser Ionization. *Anal. Chem.* **1992**, *64*, 2797−2803.

(9) Bhardwaj, C.; Hanley, L. Ion Sources for Mass Spectrometric Identification and Imaging of Molecular Species. *Nat. Prod. Rep.* **2014**, *31*, 756−767.

(10) Vekey, K. Internal Energy Effects in Mass Spectrometry. *J. Mass Spectrom.* **1996**, *31*, 445−463.

(11) Vogel, A.; Venugopalan, V. Mechanisms of Pulsed Laser Ablation of Biological Tissues. *Chem. Rev.* **2003**, *103*, 577−644.

(12) Vogel, A.; Noack, J.; Huttman, G.; Paltauf, G. Mechanisms of Femtosecond Laser Nanosurgery of Cells and Tissues. *Appl. Phys. B: Lasers Opt.* **2005**, *81*, 1015−1045.

(13) Toyran, S.; Liu, Y.; Singha, S.; Shan, S.; Cho, M. R.; Gordon, R. J.; Edwards, D. P. Femtosecond Laser Photodisruption of Human Trabecular Meshwork: An in Vivo Study. *Exp. Eye Res.* **2005**, *81*, 298−305.

(14) Kessel, L. E.; van der Poel, M.; Larsen, M. Non-Invasive Bleaching of the Human Lens by Femtosecond Laser Photolysis. *PLoS One* **2010**, *5*, e9711.

(15) Maxwell, S.; Mazur, E. Nanoprocessing of Subcellular Targets Using Femtosecond Laser Pulses. *Med. Laser Appl.* **2005**, *20*, 193−200.

(16) Nakamura, H.; Liu, Y.; Witt, T. E.; Edward, D. P.; Gordon, R. J. Femtosecond Laser Photodisruption of Primate Trabecular Meshwork: An ex Vivo Study. *Invest. Ophthalmol. Visual Sci.* **2009**, *50*, 1198−1204.

(17) Coello, Y.; Jones, A. D.; Gunaratne, T. C.; Dantus, M. Atmospheric Pressure Femtosecond Laser Imaging Mass Spectrometry. *Anal. Chem.* **2010**, *82*, 2753−2758.

(18) Milasinovic, S.; Liu, Y.; Gasper, G. L.; Zhao, Y.; Johnston, J. L.; Gordon, R. J.; Hanley, L. Ultrashort Pulse Laser Ablation for Depth Profiling of Bacterial Biofilms. *J. Vac. Sci. Technol., A* **2010**, *28*, 647−651.

(19) Cui, Y.; Moore, J. F.; Milasinovic, S.; Liu, Y.; Gordon, R. J.; Hanley, L. Depth Profiling and Imaging Capabilities of an Ultrashort Pulse Laser Ablation Time of Flight Mass Spectrometer. *Rev. Sci. Instrum.* **2012**, *83*, 093702.

(20) Milasinovic, S.; Liu, Y.; Bhardwaj, C.; Blaze M. T., M.; Gordon, R. J.; Hanley, L. Feasibility of Depth Profiling of Animal Tissue by Ultrashort Pulse Laser Ablation. *Anal. Chem.* **2012**, *84*, 3945−3951.

(21) Cui, Y.; Bhardwaj, C.; Milasinovic, S.; Carlson, R. P.; Gordon, R. J.; Hanley, L. Molecular Imaging and Depth Profiling of Biomaterials Interfaces by Femtosecond Laser Desorption Postionization Mass Spectrometry. *ACS Appl. Mater. Interfaces* **2013**, *5*, 9269−9275.

(22) Brady, J. J.; Judge, E. J.; Levis, R. J. Mass Spectrometry of Intact Neutral Macromolecules Using Intense Non-Resonant Femtosecond Laser Vaporization with Electrospray Post-Ionization. *Rapid Commun. Mass Spectrom.* **2009**, *23*, 3151−3157.

(23) Judge, E. J.; Brady, J. J.; Dalton, D.; Levis, R. J. Analysis of Pharmaceutical Compounds from Glass, Fabric, Steel, and Wood Surfaces at Atmospheric Pressure Using Spatially Resolved, Non-resonant Femtosecond Laser Vaporization Electrospray Mass Spectrometry. *Anal. Chem.* **2010**, *82*, 3231−3238.

(24) Hanley, L.; Zimmermann, R. Light and Molecular Ions: The Emergence of Vacuum UV Single-Photon Ionization in MS. *Anal. Chem.* **2009**, *81*, 4174−4182.

(25) Bhardwaj, C.; Moore, J. F.; Cui, Y.; Gasper, G. L.; Bernstein, H. C.; Carlson, R. P.; Hanley, L. Laser Desorption VUV Postionization MS Imaging of a Cocultured Biofilm. *Anal. Bioanal. Chem.* **2013**, *405*, 6969−6977.

(26) Chughtai, K.; Heeren, R. M. A. Mass Spectrometric Imaging for Biomedical Tissue Analysis. *Chem. Rev.* **2010**, *110*, 3237−3277.

(27) Römpp, A.; Schäfer, K.; Guenther, S.; Wang, Z.; Köstler, M.; Leisner, A.; Paschke, C.; Schramm, T.; Spengler, B. High-Resolution Atmospheric Pressure Infrared Laser Desorption/Ionization Mass Spectrometry Imaging of Biological Tissue. *Anal. Bioanal. Chem.* **2013**, *405*, 6959−6968.

(28) Schober, Y.; Guenther, S.; Spengler, B.; Römpp, A. High-Resolution Matrix-Assisted Laser Desorption/Ionization Imaging of Tryptic Peptides from Tissue. *Rapid Commun. Mass Spectrom.* **2012**, *26*, 1141−1146.

(29) Zavalin, A.; Todd, E. M.; Rawhouser, P. D.; Yang, J.; Norris, J. L.; Caprioli, R. M. Direct Imaging of Single Cells and Tissue at Sub-Cellular Spatial Resolution Using Transmission Geometry MALDI MS. *J. Mass Spectrom.* **2012**, *47*, 1473−1481.

(30) Nemes, P.; Barton, A. A.; Vertes, A. Three-Dimensional Imaging of Metabolites in Tissues under Ambient Conditions by Laser Ablation Electrospray Ionization Mass Spectrometry. *Anal. Chem.* **2009**, *81*, 6668−6675.

(31) Shrestha, B.; Patt, J. M.; Vertes, A. In Situ Cell-by-Cell Imaging and Analysis of Small Cell Populations by Mass Spectrometry. *Anal. Chem.* **2011**, *83*, 2947−2955.

(32) Blaze M. T., M.; Takahashi, L. K.; Zhou, J.; Ahmed, M.; Gasper, G. L.; Pleticha, F. D.; Hanley, L. Brominated Tyrosine and Polyelectrolyte Multilayer Analysis by Laser Desorption VUV Postionization and Secondary Ion Mass Spectrometry. *Anal. Chem.* **2011**, *83*, 4962−4969.

(33) Gabelica, V.; De Pauw, E. Internal Energy and Fragmentation of Ions Produced in Electrospray Sources. *Mass Spectrom. Rev.* **2005**, *24*, 566−587.

(34) Dagan, S.; Hua, Y.; Boday, D. J.; Somogyi, A.; Wysocki, R. J.; Wysocki, V. H. Internal Energy Deposition with Silicon Nanoparticle-Assisted Laser Desorption/Ionization (SPALDI) Mass Spectrometry. *Int. J. Mass Spectrom.* **2009**, *283*, 200−205.

(35) DeBord, J. D.; Verkhoturov, S. V.; Perez, L. M.; North, S. W.; Hall, M. B.; Schweikert, E. A. Measuring the Internal Energies of Species Emitted from Hypervelocity Nanoprojectile Impacts on Surfaces Using Recalibrated Benzylpyridinium Probe Ions. *J. Chem. Phys.* **2013**, *138*, 214301.

(36) Luo, G.; Marginean, I.; Vertes, A. Internal Energy of Ions Generated by Matrix-Assisted Laser Desorption/Ionization. *Anal. Chem.* **2002**, *74*, 6185−6190.

(37) Nefliu, M.; Smith, J. N.; Venter, A.; Cooks, R. G. Internal Energy Distributions in Desorption Electrospray Ionization (DESI). *J. Am. Soc. Mass Spectrom.* **2008**, *19*, 420−427.

(38) Nemes, P.; Huang, H.; Vertes, A. Internal Energy Deposition and Ion Fragmentation in Atmospheric-Pressure Mid-Infrared Laser Ablation Electrospray Ionization. *Phys. Chem. Chem. Phys.* **2012**, *14*, 2501−2507.

(39) Lim, Y. C.; Johnson, J.; Fei, Z.; Wu, Y.; Farson, D. F.; Lannutti, J. J.; Choi, H. W.; Lee, L. J. Micropatterning and Characterization of Electrospun Poly(ε-caprolactone)/Gelatin Nanofiber Tissue Scaffolds by Femtosecond Laser Ablation for Tissue Engineering Applications. *Biotechnol. Bioeng.* **2011**, *108*, 116−126.

(40) Amoruso, S.; Ausanio, G.; Barone, A. C.; Bruzzese, R.; Gragnaniello, L.; Vitiello, M.; Wang, X. Ultrashort Laser Ablation of Solid Matter in Vacuum: A Comparison between the Picosecond and Femtosecond Regimes. *J. Phys. B* **2005**, *38*, L329−L338.

(41) Oguri, K.; Okano, Y.; Nishikawa, T.; Nakano, H. Dynamics of Femtosecond Laser Ablation Studied with Time-Resolved X-Ray Absorption Fine Structure Imaging. *Phys. Rev. B* **2009**, *79*, 144106.

(42) Husinsky, W.; Dachraoui, H. Velocity Distribution of Neutral Particles Ejected from Biological Material under Ultra Short Laser Radiation. *arXiv.org, e-Print Arch., Phys.* **2012**, No. arXiv:1201.4966.

(43) Kostko, O.; Takahashi, L. K.; Ahmed, M. Desorption Dynamics, Internal Energies and Imaging of Organic Molecules from Surfaces with Laser Desorption and Vacuum Ultraviolet (VUV) Photo-ionization. *Chem.—Asian J.* **2011**, *6*, 3066−3076.

(44) Zhigilei, L. V.; Leveugle, E.; Garrison, B. J.; Yingling, Y. G.; Zeifman, M. I. Computer Simulations of Laser Ablation of Molecular Substrates. *Chem. Rev.* **2003**, *103*, 321−347.

(45) Knochenmuss, R.; Zhigilei, L. V. Molecular Dynamics Simulations of MALDI: Laser Fluence and Pulse Width Dependence of Plume Characteristics and Consequences for Matrix and Analyte Ionization. *J. Mass Spectrom.* **2010**, *45*, 333−346.

(46) Gamaly, E. G.; Rode, A. V.; Luther-Davies, B. Ablation of Solids by Femtosecond Lasers: Ablation Mechanism and Ablation Thresh-olds for Metals and Dielectrics. *Phys. Plasmas* **2002**, *9*, 949−957.

(47) Feit, F. D.; Rubenchik, A. M.; Kim, B.-M.; Da Silva, L. B.; Perry, M. D. Physical Characterization of Ultrashort Laser Pulse Drilling of Biological Tissue. *Appl. Surf. Sci.* **1998**, *127−129*, 869−874.

(48) Kim, B.-M.; Feit, F. D.; Rubenchik, A. M.; Joslin, E. J.; Eichler, J.; Stoeller, P. C.; Da Silva, L. B. Effects of High Repetition Rate and Beam Size on Hard Tissue Damage Due to Subpicosecond Laser Pulses. *Appl. Phys. Lett.* **2000**, *76*, 4001−4003.

(49) Collettee, C.; Drahos, L.; De Pauw, E.; Vekey, K. Comparison of the Internal Energy Distributions of Ions Produced by Different Electrospray Ionization Sources. *Rapid Commun. Mass Spectrom.* **1998**, *12*, 1673−1678.

(50) Guenther, S.; Koestler, M.; Schulz, O.; Spengler, B. Laser Spot Size and Laser Power Dependence of Ion Formation in High Resolution MALDI Imaging. *Int. J. Mass Spectrom.* **2010**, *294*, 7−15.

28947

dx.doi.org/10.1021/jp504062u | *J. Phys. Chem. C* 2014, 118, 28938−28947